Available online at www.sciencedirect.com
SCIENCE DIRECT
Journal of Power Sources 154 (2006) 327–342
JOURNAL OF POWER SOURCES
www.elsevier.com/locate/jpowsour

The potential of model studies for the understanding of catalyst poisoning and temperature effects in polymer electrolyte fuel cell reactions

R.J. Behm *, Z. Jusys

Department of Surface Chemistry and Catalysis, University of Ulm, D-89069 Ulm, Germany

Available online 15 December 2005

Abstract

In this contribution we demonstrate the potential of model studies for the understanding of electrocatalytic reactions in low-temperature polymer electrolyte fuel cells (PEFCs) operated by H_2-rich anode feed gas, in particular of the role of temperature effects and catalyst poisoning. Reviewing previous work from our laboratory and, for better comparison, focussing on carbon-supported Pt catalysts, the important role of using fuel cell relevant reaction and mass transport conditions will be outlined. The latter conditions include continuous reaction, elevated temperatures, realistic supported catalyst materials and controlled mass transport. The data show the importance of combining electrochemical techniques such as rotating disc electrode (RDE), wall-jet and flow cell measurements, and on-line differential electrochemical mass spectrometry (DEMS) under controlled mass transport conditions.

Keywords: Polymer electrolyte fuel cell; H_2/CO_2 oxidation; Air bleed; Catalyst poisoning; Temperature effects; Model studies

1. Introduction

Catalyst poisoning and temperature effects are of outmost interest for the operation of low-temperature polymer electrolyte fuel cells (PEFCs): Catalyst poisoning is one of the main electrocatalytic problems for the efficiency and long-term operation of low-temperature PEFCs, and increasing the operating temperature is one of the main strategies for improving the performance of PEFCs, which also provides the driving force for the large efforts in developing suitable, more temperature resistant membranes with sufficient proton conductivity [1,2].

It is generally realized that catalyst poisoning leads to a reduction of the catalytic activity of the catalyst, by blocking part of the surface of the active component ('active sites'), which results in a lower power density of the fuel cell [3,4]. This is, however, not the only way of affecting the catalyst performance. Other possible effects include, e.g., changes in the selectivity, which may also affect the performance of the fuel cell. Another and in some cases even more important consequence may be the formation of undesirable side products. One important example is the formation of H_2O_2 during air bleed operation of PEFC anode catalysts, which may have devastating consequences for the long-term stability of the membrane [5–8]. Operation at increased temperatures will not only allow to exploit the inherent increase of the reaction rate at higher temperatures in thermally activated reactions, it may also reduce the effect of adsorbed catalyst poisons, which may, at least partly, be removed by thermal desorption under these conditions. Removal of catalyst poisons by thermal desorption rather than by the commonly discussed reactive removal, by electrooxidation or by chemical reaction as for instance in the so-called air bleed operation [9], is not limited to weakly adsorbed catalyst poisons, but may play an important role also for adsorbates such as adsorbed CO (CO_{ad}), which are considered as strongly chemisorbed (see below), at room temperature and above. Hence, understanding of the physical origin of catalyst poisoning will also affect the strategies for the development of improved catalysts, aiming perhaps at improved CO_{ad} desorption rather than improved CO_{ad} oxidation in the case of CO tolerant anode catalysts, where the first would result from reduced adsorption energies, while the second is caused by improved OH_{ad} formation (water splitting).

The results of both different catalyst poisons and of increasing temperature can clearly be observed in fuel cell performance measurements. These measurements, however, rarely allow an unambiguous and quantitative analysis of the catalytic effects related to the variation in fuel cell performance because of the

* Corresponding author.
E-mail address: juergen.behm@chemie.uni-ulm.de (R.J. Behm).

0378-7753/$ – see front matter © 2005 Elsevier B.V. All rights reserved.
doi:10.1016/j.jpowsour.2005.10.086

complex and often ill-defined transport conditions and reaction kinetics (catalyst utilization, water management, etc.) in a fuel cell. Better access to these effects is possible in electrocatalytic model studies, where the reaction conditions are much simpler and better defined than during fuel cell operation. On the other hand, these model studies are often performed under conditions and on model catalysts which are so different from fuel cell operating conditions and materials that it is questionable in how far their results can be transferred to the situation in an operating fuel cell. We have therefore started a series of studies on materials and under reaction conditions, which are as closely as possible related to fuel cell operating conditions, while still being sufficiently well defined for a clear evaluation of the (electro-)catalytic effects [6,7,10–36]. This includes (i) the use of carbon-supported catalysts identical to those used for PEFC electrode preparation, however, at well-defined catalyst loading and up to 100% utilization of the active (surface) sites in a thin-film electrode, (ii) measurements under continuous reaction and continuous electrolyte flow conditions with well-defined mass transport properties, and (iii) measurements at elevated temperatures.

We will limit the present overview to effects relevant for H_2 and reformate operated PEFCs. Catalyst poisoning and temperature effects in reactions relevant for the operation of PEFCs via oxidation of organic fuels such as the direct methanol fuel cell (DMFC) or the direct ethanol fuel cell (DAFC) will not be considered (for further details on these reactions see Refs. [20,24,26,28,30–36]). We will, from reasons of simplicity, concentrate mostly on results of our own work, though results of other groups and on other model systems will be included in the discussion. Furthermore, we will focus on reaction effects observed for carbon-supported Pt catalysts in order to allow a systematic evaluation and comparison of these effects. Data on other carbon-supported and unsupported catalysts will be given for comparison.

In the following we will first discuss the role of reaction conditions and catalyst materials for the relevance of model studies for the understanding of fuel cell reactions and fuel cell operation. This is followed by a brief evaluation of the different sources for catalyst poisons during fuel cell operation. In the main part we will demonstrate the effect of different catalyst poisons on the activity and selectivity of fuel cell catalysts in H_2 or reformate operated PEFCs, using CO and CO_2 poisoning and the (very different) effect of these poisons on the hydrogen oxidation reaction (HOR) as examples. In the context of CO poisoning we will elucidate the effect of increasing reaction temperature as well as electrocatalytic aspects of the so-called air bleed operation of PEFCs fed by reformate. Finally we will present and discuss data on the long-term stability and deactivation of Pt/Vulcan electrodes under anodic and cathodic reaction conditions, respectively, which demonstrate the much higher sensitivity of the anode catalyst towards poisoning by adsorption of trace impurities compared to the cathode catalyst. In total, the data clearly demonstrate (i) the impact and decisive role of the reaction temperature on the characteristics of low temperature fuel cells and (ii) the impact of catalyst poisoning. They furthermore underline the value of model studies for the understanding of electrocatalytic reactions in low temperatures fuel cells, but also the importance of applying adequate, fuel cell relevant reaction and transport conditions and using appropriate catalyst materials.

2. Relevance of model studies for the understanding of fuel cell reactions

As mentioned above electrocatalytic model studies have the clear advantage of a more direct interpretation and assignment of the kinetic and spectroscopic results compared to measurements in real fuel cells, even in single cell laboratory models.

Experimentally most simple and also most common are potentiodynamic studies of electrocatalytic reactions on massive bulk electrodes, either single-crystalline or polycrystalline samples, in resting electrolyte and at room temperature. These measurements, however, suffer from the ill-defined transport and diffusion conditions, and also from the convolution of time effects and potential effects during the potential scan. These deficiencies are avoided by measurements under defined transport conditions, e.g., in flow cell measurements [37–40], in wall-jet electrode measurements [41–44] or in rotating disk electrode (RDE) measurements [45–47], and by performing measurements under continuous reaction conditions and at constant potential (potentiostatic measurements). Temperature effects have been investigated by raising the reaction temperature in these model studies. Due to increasing electrolyte evaporation this is limited, however, to temperatures between 60 and 80 °C in an open reaction vessel. Therefore, several groups have developed flow cell set-ups which can be pressurized and hence can operate also at higher temperatures, up to 120 °C [40,48]. Finally, the transition to more realistic materials was made by going to recast electrodes [49,50] or to thin-film supported catalyst electrodes, where a thin film of carbon-supported catalyst (thickness approximately 1 μm) is deposited on a planar glassy carbon stub and mechanically fixed by a very thin Nafion film deposited from an aqueous Nafion solution (ca. 0.1 μm thickness) [10]. After mounting in an RDE configuration we used these thin-film model electrodes in numerous kinetic studies [10–17,25]. These electrodes are already close to a realistic fuel cell configuration and offer the advantage that the Nafion film is sufficiently thin that it does not cause any significant diffusion resistance. Therefore, the measured reaction kinetics directly reflect the electrocatalytic reaction kinetics and complex modeling, which is otherwise necessary in order to extract the reaction kinetics [51], can be avoided.

Basically all model studies generally differ from realistic fuel cell measurements in that they are performed in liquid electrolyte rather than at the three-phase boundary between catalyst, solid electrolyte (membrane) and feed gas. Thus, the model studies are free from complications due to water management (drying of the membrane, flooding of the catalyst layer, etc. [52]), which can largely contribute to the fuel cell performance under realistic conditions. On the other hand, effects from anion adsorption may play a significant role in model studies in liquid electrolyte, in contrast to a fuel cell surrounding, where anions are present only as sulfonic acid groups in the polymer membrane. Though in our

studies the catalyst layer is covered by a thin Nafion film, anions can more or less freely access the catalyst surface. In order to reduce anion effects, a number of studies used $HClO_4$ solution instead of the more commonly applied H_2SO_4 solution as base electrolyte [25,50,53–56].

Next, these model studies also offer the advantage to apply modern spectroscopic techniques such as in situ IR or on-line mass spectrometry (differential electrochemical mass spectrometry (DEMS)), just to name the most important ones. The rich information that can be derived from these techniques has been demonstrated in numerous studies [6,7,18–24,26–36,57–62]. From the same reasons as discussed above it would be desirable to apply these techniques under realistic conditions and on fuel cell relevant materials. In both cases, however, the majority of these studies have been performed under conditions which render a direct comparison with fuel cell processes difficult. In situ IR studies have almost exclusively been performed on massive noble metal electrodes, using IR reflection absorption spectroscopy (IRRAS) techniques in a thin-layer configuration, where the electrode is pressed against an optical prism in order to reduce absorption in the electrolyte, and the incoming IR beam has to pass through the thin electrolyte film (thickness $\leq 10\ \mu m$) between prism and electrode before and after being reflected at the electrode [62]. Under these conditions mass transport in the thin-layer gap is practically inhibited, leading to a depletion of reactants as well as accumulation and possibly readsorption of by-products, which can result in strongly misleading conclusions, in particular for continuous electrocatalytic reactions [62]. These limitations can be largely reduced by performing the measurements in an attenuated total reflection (ATR) configuration [63,64], where a thin metal film deposited on an optical prism serves as a working electrode and the IR beam is transmitted internally from the back side of the prism to the film and totally reflected at the prism|film interface. In this technique the working electrode is freely accessible to the electrolyte, reducing the transport limitations [64]. Furthermore, the use of nanostructured, porous films prepared by electroless deposition leads to significant surface enhancement effects and hence higher signal intensities (surface-enhanced absorption reflection spectroscopy (SEIRAS)) [64]. First studies on the oxidation of organic molecules on Pt films demonstrated the potential of this technique [34,35,65–67]. Well-defined transport conditions are obtained when coupling this configuration with a flow cell set-up, as it had been described recently [68].

More realistic from the materials side are a few IRRAS studies on the electrocatalytic behavior of supported catalyst layers, which were deposited, e.g., on catalytically inert, reflecting Au [69,70] or glassy carbon [70–73] electrodes. A next step to be done is the transition to more realistic electrode materials (carbon-supported fuel cell catalysts) also in a SEIRAS configuration.

Early DEMS measurements mostly used porous electrodes, which were painted or sputtered on the membrane separating the electrochemical cell from the vacuum side with the mass spectrometer [74]. These porous films have the disadvantage that the complete exchange of electrolyte is slow and that remnants of the initial reactant containing electrolyte may remain in the pores of the porous metal layer, which would affect, e.g., the result of adsorbate stripping experiments. Furthermore, also the collection efficiency may be changed significantly modified. Both effects will affect the conclusions on the nature of adsorbed reaction intermediates present on the electrode before adsorbate stripping. Therefore it is not astonishing that later studies using different electrode configurations came to different conclusions on the reaction mechanism and adsorbed reaction intermediates than these early studies [20,75]. An important improvement for the current purposes was the development of a flow cell for on-line DEMS measurements, which allowed to perform DEMS studies on massive electrodes under continuous electrolyte flow and hence under well-defined diffusion conditions [76]. Subsequently, we have modified this flow-cell set-up such that it could be combined with the thin-film supported catalyst electrodes described above [21,77,78]. This set-up has largely been used in our own studies. Due to the high sensitivity of this set-up we could not only follow the formation of volatile reaction products, but also the consumption of gaseous and volatile liquid reactants. Using proper calibration methods this allowed to determine the amount of adsorbed species in real time, during the adsorption process, which could be used, e.g., to directly correlate the catalytic activity with the coverage of specific adsorbates. For instance, this technique was applied to quantitatively determine the effect of a CO adlayer on the activity of a supported Pt/Vulcan catalyst for H_2 oxidation [21] or for O_2 reduction [6] as a function of CO_{ad} coverage.

In situ spectroscopy methods were applied also in studies of specially designed fuel cells, allowing in situ IR studies in an operating PEFC [79,80] and on-line DEMS detection in the exhaust of a fuel cell [81–85]. The particular value of these developments is that they extend the range of detailed chemical information to fully realistic configurations and reaction conditions, and hence enable one to relate the mechanistic information derived in model studies under defined conditions to these realistic conditions.

Finally it is important to note that model studies under defined mass transport conditions determine the kinetic limit of a given reaction, at least in simple reactions. Additional mass transport limitations, both for fuel transport and for removal of poisons, will generally result in lower reaction rates. Hence, comparison of the (catalyst mass normalized) reaction rates in a fuel cell with these kinetic limits allows to estimate, whether the respective reaction is limited by mass transport or other design related effects, or by the inherent reaction kinetics of the catalyst.

3. Origins of catalyst poisons

Catalyst poisons can originate from different sources: (i) they are carried into the fuel cell as contaminations in the feed stream, (ii) they result from internal sources, mainly from components of the electrodes or the membrane or from corrosion/decomposition products of these parts, or (iii) they reach the electrode by cross-over from the respective other electrode compartment [25]. Furthermore, we have to distinguish between anode and cathode poisoning, since due to the very different

reaction (potential) conditions these will be differently affected by the same species.

Most commonly, fuel cell catalyst poisoning is associated with CO adsorption on the anode catalyst, which had been investigated extensively (see [21,86] and references therein). CO is present in H_2-rich fuel gases generated by reforming and/or partial oxidation of various hydrocarbons, in particular of natural gas, gasoline, methanol or higher alcohols (reformate gas) [87]. In addition to CO also other contaminations or regular components in the feed gas can act as catalyst poison. In the anode feed stream this includes, e.g., CO_2, which depending on the original energy carrier may contribute by 20% or more to reformate gases [88–90], unless it is removed from the feed gas by sequestration [87]. The other major component in reformate gases, H_2O, is commonly treated in the water household of a fuel cell, but strictly speaking the water vapor content will also affect the catalytic properties of the anode catalyst. In this overview we will not include it from the simple reason that the model studies discussed below are performed in aqueous solution. Other potential catalyst poisons in the feed stream include CH_4 or common air impurities such as SO_x, NO_x or H_2S or NH_3. Sulfur and sulfur containing molecules are known as very efficient catalyst poisons on noble metal catalysts, which lead to significant degradation of the fuel cell performance and hence have to be removed before entering the fuel cell [91–93]. Similar, but less pronounced effects have been reported for NO_2 [93]. First studies on different metals/catalysts on the influence of trace impurities of ammonia in the anode feed gas showed significant performance losses in the presence of trace impurities (1–10 ppm) of NH_3 in the anode feed gas [94,95]. NH_3 was found to affect H adsorption, shifting it to lower potentials [95,96]. Significant effects were also observed for the ORR on the cathode. Under these conditions NH_3 oxidation is active, leading to N_2, NH_x,ad or NO_x species, the potential for NH_{ads} or N_{ads} was found to depend on the nature of the metal [97].

The second class includes catalyst poisons resulting from corrosion and leaching of membrane and other fuel cell or periphery components. Possible examples for this are hydrocarbon contaminants dissolved from the MEA or metal ions resulting from corrosion processes. Hydrocarbons are likely to be removed from the cathode catalyst by oxidation processes, but are stable under anode reaction conditions. The same is true for many metallic deposits resulting from periphery corrosion processes. Therefore we can expect that such catalyst poisoning effects are much more severe on the anode than on the cathode due to the low operating potential. Note that this is opposite to electrode corrosion processes, which based on the reaction conditions should be much more pronounced on the cathode than on the anode side.

In the third class, we summarize catalyst poisons resulting from cross-over via the membrane. The most common example is that of methanol cross-over from the anode to the cathode in methanol fuel cells [98–100]. Less often discussed, but presumably also important, is O_2 cross-over from the cathode to the anode [101], which may play an important role for the removal of oxidizable contaminants from the anode catalyst by chemical reaction, but also for the generation of H_2O_2 at the anode via O_2 reduction at anode operating potentials (see below).

The same is true for H_2 cross-over from anode to cathode [102]. In addition, metal ions (resulting from corrosion) and ammonium ions (due to NH_3 contamination) diffusing into the membrane can reduce the proton conductivity of the membrane [94].

4. Results and discussion

4.1. CO adsorption and H_2 oxidation in CO/H_2 mixtures on Pt/Vulcan and PtRu/Vulcan supported catalyst

4.1.1. H_2 oxidation on a CO_{ad} covered Pt/Vulcan supported catalyst

H_2 oxidation in the presence of CO is the most extensively studied case of a poisoning effect, both in fuel cell measurements and in model studies on various types of model electrodes [86]. Based on the observation that H_2 oxidation proceeds with considerable rates even in the presence of significant amounts of adsorbed CO [9,103], Gottesfeld and coworkers proposed a mechanism where H_2 oxidation, via dissociation to H_{ad} [103] and subsequent desorption as H^+, can take place in fluctuating holes of the CO adlayer [9,104]. Later on, this model was adopted also by other authors [87,105–109]. Because of the high rate (high exchange current density) of the HOR this results in considerable currents even on a small fraction of the active surface.

From the same reason the HOR current is largely limited by transport effects on a clean surface. Otherwise a reduction of the active surface, as it is found for a partly CO_{ad} covered catalyst surface, should result at best in a linear decay of the HOR activity with increasing relative CO_{ad} coverage $\theta_{CO,rel}$ ($\theta_{CO,rel}$ is defined as $\theta_{CO,rel} = 1$ at CO_{ad} saturation), if the catalyst surface area accessible for the HOR is given by $1 - \theta_{CO,rel}$ and if the rate of the HOR is simply determined by the surface area available for it (first order adsorption kinetics [110]).

A quantitative relation between CO_{ad} coverage and HOR activity on a carbon-supported Pt catalyst was derived recently by on-line DEMS experiments, following the HOR current and loss in H_2 partial pressure as a function of CO_{ad} coverage during CO adsorption/H_2 oxidation from/in a 2%CO/H_2 mixture [21]. It should be noted that under reaction conditions the Pt catalyst is initially covered by a H-upd adlayer, which, however, is weakly adsorbed and does not hinder the uptake of CO [21]. As shown in Fig. 1c and a, the CO^+ related mass spectrometric signal indicative of the CO partial pressure in the 2%CO/H_2-saturated electrolyte remains at a low level due to CO adsorption when stepping the potential of the Pt/Vulcan catalyst electrode from 1.2 V_{RHE} (CO oxidation) to 0.06 V_{RHE} (CO adsorption), while the HOR current initially assumes the mass transport limited current value [111]. Subsequently both the CO (Fig. 1c) and H_2 partial pressure (H_2^+ related mass spectrometric signal in Fig. 1b) increase steadily, mirroring the Faradaic current decrease (Fig. 1a), and finally assume the steady-state value characteristic for complete poisoning, with no CO/H_2 consumption at the electrode and zero current flow. By integrating

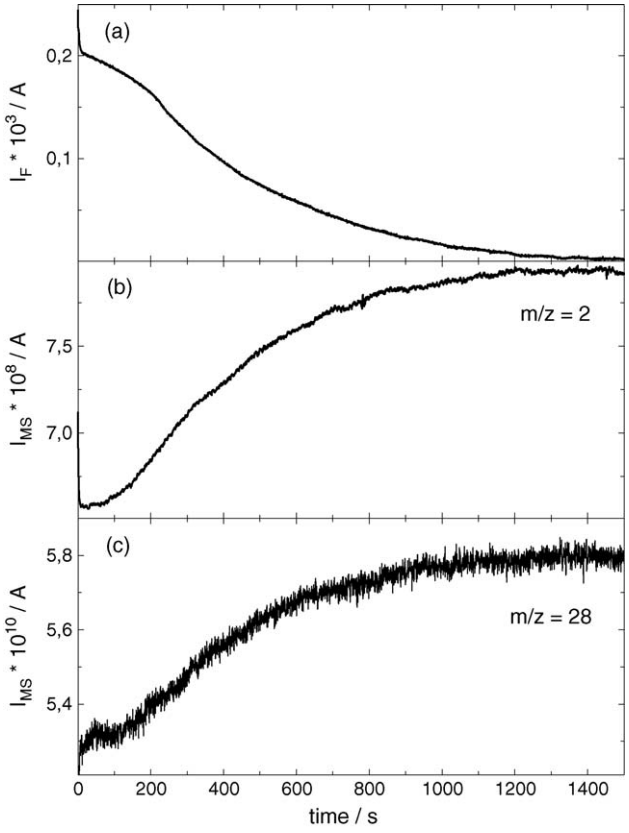

Fig. 1. Faradaic current (a) and mass spectrometric signals of the H_2 partial pressure ($m/z = 2$) (b) and of the CO partial pressure ($m/z = 28$) (c) during CO adsorption/H_2 oxidation on a 20 wt.% Pt/Vulcan catalyst electrode (Pt loading 28 μg cm^{-2}) in 2%CO/H_2-saturated 0.5 M H_2SO_4 solution (room temperature, 0.06 V_{RHE}, at $t = 0$ s the potential was stepped from 1.2 V_{RHE} to 0.06 V_{RHE}) (with permission from Ref. [21]).

the amount of consumed CO with time and normalizing to the total amount of consumed CO [21], we obtain a relation between relative CO_{ad} coverage and adsorption time. Based on this relation we can directly determine the H_2 consumption, which is directly related to the HOR current, as a function of CO coverage. This relation is reproduced as dotted line in Fig. 2. For comparison we also include the normalized electrochemical current measured during this experiment (full line), which largely exhibits similar characteristics. Small deviations are attributed to capacitive contributions to the Faradaic current and H-upd displacement. Clearly, the HOR current does not at all decay linearly with increasing CO_{ad} coverage (dashed line), or even less with $(1 - \theta_{CO})^2$, which would be applicable for second order Langmuir adsorption kinetics. Instead, the decay of the HOR current is much slower, in good agreement with previous, qualitative reports [12,103]. Since we know from potentiodynamic measurements that at 0.06 V_{RHE} reaction potential the HOR rate in our flow cell configuration and at present electrolyte flow is transport limited [21], the observation of an initially slow, nonlinear decay of the HOR current with CO_{ad} coverage agrees well with a hypothesis that these characteristics are, at least partly, due to transport limitations. Finally, we want to note that the CO consumption at any given adsorption time (or CO_{ad} coverage) reflects the effective probability for CO to be adsorbed on

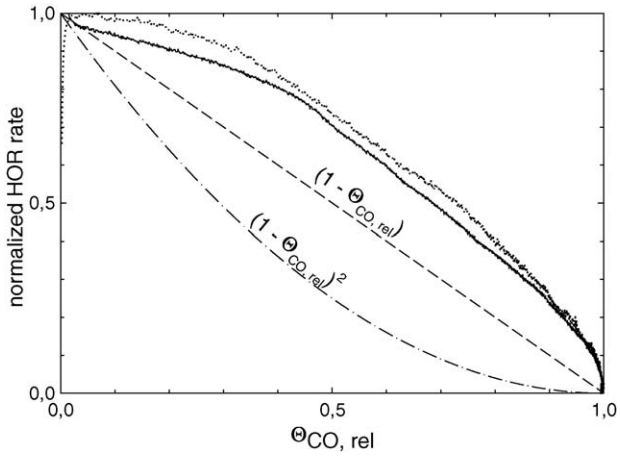

Fig. 2. Faradaic current (full line) and H_2 consumption (dotted line) as a function of the relative CO coverage, $\theta_{CO,rel}$. For comparison, we also include the relations expected for a linear relation (dashed line, first order Langmuir adsorption kinetics) and a $(1 - \theta)^2$ relation (dash-dotted line, second order Langmuir adsorption kinetics) between HOR activity and CO_{ad} coverage (with permission from Ref. [21]).

the partly CO_{ad} covered catalyst while passing through the flow cell. It should be noted that this probability is closely related to, but not identical to the so-called 'sticking coefficient', which describes the probability of a gas particle, in this case of the CO molecule, to adsorb when hitting a smooth surface in a single incident [110,112]. A plot of this effective adsorption probability versus the CO_{ad} coverage (not shown here) reveals that this probability remains rather constant in the low and medium CO_{ad} coverages, while most of the decay occurs at higher coverages [21].

In total these measurements confirm on a quantitative scale previous observations that H_2 oxidation is possible and occurs at significant rates even on Pt surfaces covered by relatively dense CO adlayers [87,103,106–109]. On a microscopic scale the HOR current–CO_{ad} coverage relation in Fig. 2 can be explained either transport limitations in the low CO_{ad} coverage regime, by readsorption effects and/or by a precursor like behavior, where the H_2 molecule can spend some time on the CO_{ad} covered Pt surface and perform several attempts for dissociative adsorption before it is finally transported away from the surface [113,114]. Readsorption effects describe the increased probability for adsorption or reaction of a particle within the catalyst layer due to the fact that, after an unsuccessful adsorption attempt, it will experience several collisions with the active surface of Pt particles before it will finally leave this layer and diffuse away. This is schematically displayed in Fig. 3. The latter two reaction schemes would lead to an increased reaction probability in the medium and higher CO_{ad} coverage regime compared to a linear HOR current–CO_{ad} coverage behavior.

4.1.2. Temperature effects on CO oxidation and H_2 oxidation on a partly CO_{ad} covered Pt/Vulcan supported catalyst

It is well known from various fuel cell measurements that at a given CO partial pressure and amount of noble metal catalyst the effect of CO_{ad} poisoning on the HOR rate depends

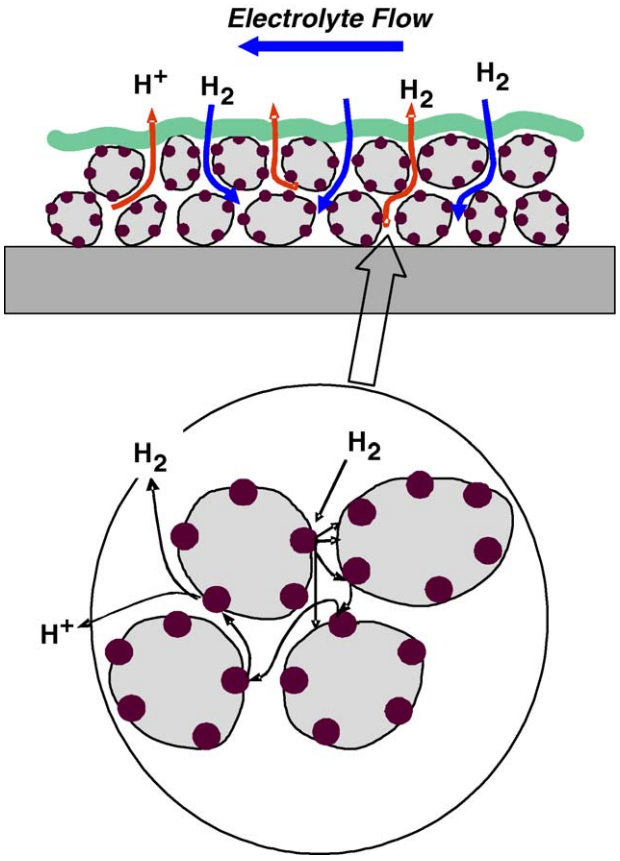

Fig. 3. Schematic description of readsorption effects in the catalyst layer. Reactive molecules will encounter several collisions with active catalyst molecules before they will finally leave the catalyst layer. If each collision has a probability of $(1-\theta)$ for successful adsorption (first order Langmuir adsorption kinetics), where θ denotes the coverage of a site blocking adsorbate, the total probability of the incoming molecule to adsorb/react in the catalyst layer will be higher than that. The exact value will depend on the number of collisions before leaving the catalyst layer.

sensitively on the operating temperature [2,115]. This may result from different effects: (i) the inherent increase of the HOR rate with temperature, (ii) an acceleration in OH_{ad} formation and subsequent CO_{ad} oxidation, by reaction with OH_{ad}, and/or (iii) a reduction in steady-state CO_{ad} coverage due to increasing thermal desorption. Previous studies reported that the CO_{ad} coverage decays between room temperature and about 70–80 °C [115–120], based on the decay in CO_{ad} stripping charge [115,118–120] or in situ IR spectroscopy measurements [116,117]. In these measurements it cannot be excluded, however, that the CO coverage is reduced due to CO desorption between adsorption and stripping, which often requires significant time due to the necessity of removing the CO from the electrolyte. More detailed stripping studies of the temperature dependence showed that CO desorption starts at about 50 °C on single-crystalline Pt surfaces [118,119] or at 50–60 °C on carbon-supported Pt catalysts [120,121].

In order to investigate these effects in more detail and to discriminate between CO_{ad} coverage and temperature effects we studied the CO_{ad} stripping behavior on a Pt/Vulcan catalyst electrode in base electrolyte and in 2%CO/H_2-saturated electrolyte as a function of adsorption/stripping temperature, recording both the Faradaic current and the $m/z = 44$ mass spectrometric current. Prior to these measurements we examined effects of the CO_{ad} coverage, e.g., by blocking sites for H_2O adsorption and OH_{ad} formation, by performing CO_{ad} stripping experiments after controlled adsorption of different amounts of CO at room temperature. It should be noted that in our flow cell measurements the time required for electrolyte exchange is by far shorter than typical times necessary for removing CO from a stagnant electrolyte, e.g., by purging with Ar. As shown in Fig. 4, both the Faradaic current and the mass spectrometric signal exhibit the typical shape of the CO stripping signal from Pt/Vulcan catalyst electrodes [21] and increase in intensity with CO_{ad} coverage. The small potential shift of the peak maximum with increasing CO_{ad} coverage, from 0.785 V_{RHE} at $\theta_{CO,rel} = 1.0$–0.745 V_{RHE} at $\theta_{CO,rel} = 0.15$, and the almost CO_{ad} coverage independent onset potential indicate that CO_{ad} oxidation is not limited by site blocking effects, where the CO adlayer inhibits water splitting by blocking the necessary adsorption sites. It is rather determined by the inherent kinetic limitations for water splitting and subsequent oxidation of the CO_{ad} species. Our data agree well with previous reports for CO_{ad} stripping on Pt single crystal surfaces and carbon-supported Pt catalyst, which equally found only small shifts in the CO_{ad} stripping peak position with increasing CO coverage [122–124]. It should be noted that the potential shifts are much more pronounced if the CO_{ad} coverage is varied by oxidative removal of part of a saturated CO adlayer [105], which most likely is related to a different structure/lateral distribution of adlayer. Different stripping characteristics are obtained also if the CO adlayer is produced by dissociative adsorption of methanol [20,125] or by reductive

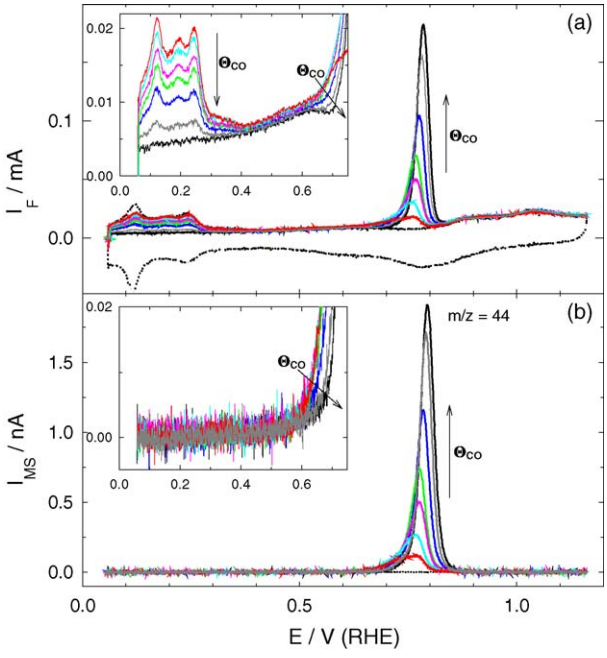

Fig. 4. Faradaic current (a) and mass spectrometric ($m/z = 44$) (b) signal for CO stripping from a carbon-supported Pt/Vulcan catalyst electrode in pure base electrolyte (7 $\mu g_{Pt}\,cm^{-2}$), after adsorption of increasing amounts of CO from CO-saturated 0.5 M H_2SO_4 solution (scan rate 10 mV s^{-1}, room temperature).

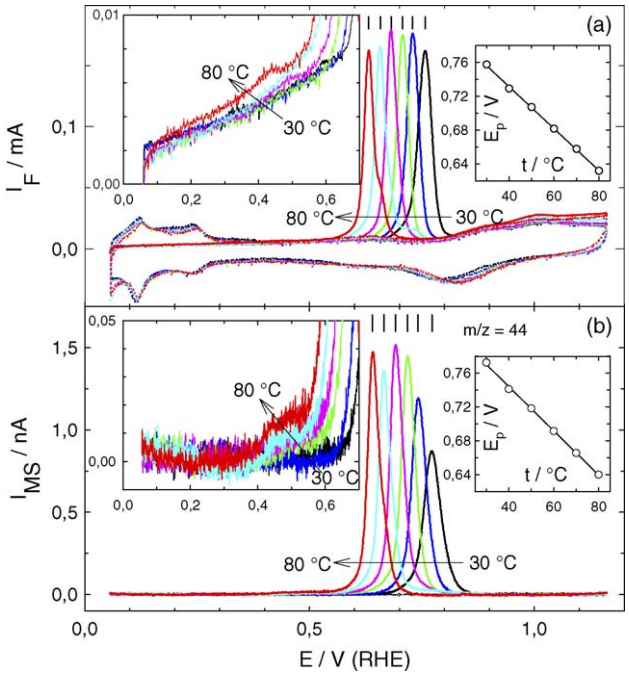

Fig. 5. Faradaic current (a) and mass spectrometric ($m/z = 44$) (b) signal for CO stripping from a CO_{ad} saturated carbon-supported 20 wt.% Pt/Vulcan catalyst electrode (7 $\mu g_{pt}\,cm^{-2}$) at different temperatures in pure base electrolyte, after adsorption of CO from CO-saturated 0.5 M H_2SO_4 solution for 5 min at the respective temperatures (temperatures: 30, 40, 50, 60, 70, and 80 °C, scan rate 10 mV s^{-1}).

adsorption of CO_2 at cathodic potentials [75] rather than by adsorption of CO.

The picture is completely different when looking at the effect of increasing adsorption/oxidation temperatures, which was examined by stripping of a saturated CO adlayer on a Pt/C catalyst electrode (Fig. 5). In this case the CO_{ad} stripping peaks exhibit a significant shift to lower potentials, from 0.76 V at 30 °C to 0.64 V at 80 °C, and also a slight narrowing of the main peak, from 0.10 V at 30 °C (FWHM) to 0.08 V at 80 °C. In addition to the shift of the main peak also the low potential pre-wave changes with temperature, by shifting its onset to lower potentials with increasing temperature, from 0.4 V at room temperature to about 0.3 V at 80 °C. Clearly, these shifts do not result from a temperature induced lowering of the coverage (see below), but reflect the activation barrier for water splitting and/or CO_{ad} oxidation.

The linear negative shift in peak potential with increasing adsorption/oxidation temperature closely resembles findings for CO adsorption/stripping on single-crystalline Pt surfaces [118,119], even on a quantitative scale. Those authors derived an activation barrier of 132 kJ mol^{-1} for CO oxidation on Pt(1 1 1) in sulfuric acid solution, within the limits of their model assumptions. Considering the close similarity of our data, the CO oxidation barrier on Pt/C catalyst must be close to this value.

The variation in CO_{ad} coverage with increasing temperature, as determined from the $m/z = 44$ peak charge (for details see [21]), is illustrated in Fig. 6. While at temperatures up to around 50–60 °C the coverage is almost constant, with values around $\theta_{CO,rel} = 0.95$, higher adsorption/reaction temperatures result in

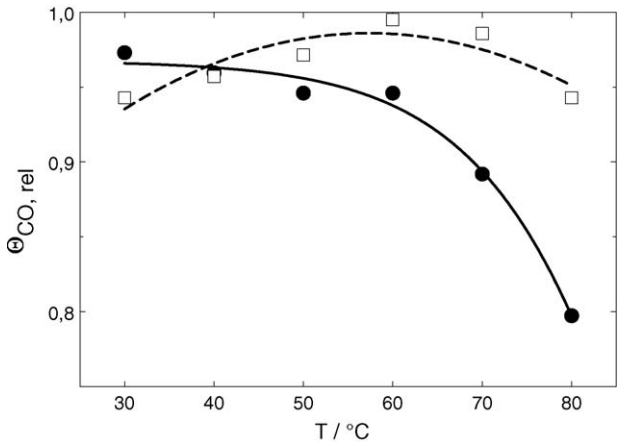

Fig. 6. Evolution of the CO_{ad} saturation coverage on a carbon-supported Pt/Vulcan catalyst electrode after adsorption of CO from CO-saturated 0.5 M H_2SO_4 solution (full symbols, stripping in inert base electrolyte, data from Fig. 5) and from 2%CO/H_2-saturated 0.5 M H_2SO_4 solution (empty symbols, stripping in 2%CO/H_2-saturated electrolyte, data from Fig. 7) for 5 min at the respective temperatures.

a significant reduction of the CO_{ad} coverage to $\theta_{CO,rel} = 0.9$ at 70 °C and $\theta_{CO,rel} = 0.8$ at 80 °C. This is attributed to thermal desorption of CO_{ad} in the time period between CO adsorption and CO_{ad} stripping (ca. 5 min for complete electrolyte exchange for our thin-layer flow cell).

More relevant for fuel cell applications is the effect of increasing temperature on the HOR in the presence of CO in the feed gas and hence in the presence of a CO adlayer. This is illustrated in Fig. 7, which shows CO_{ad} stripping signals recorded from a

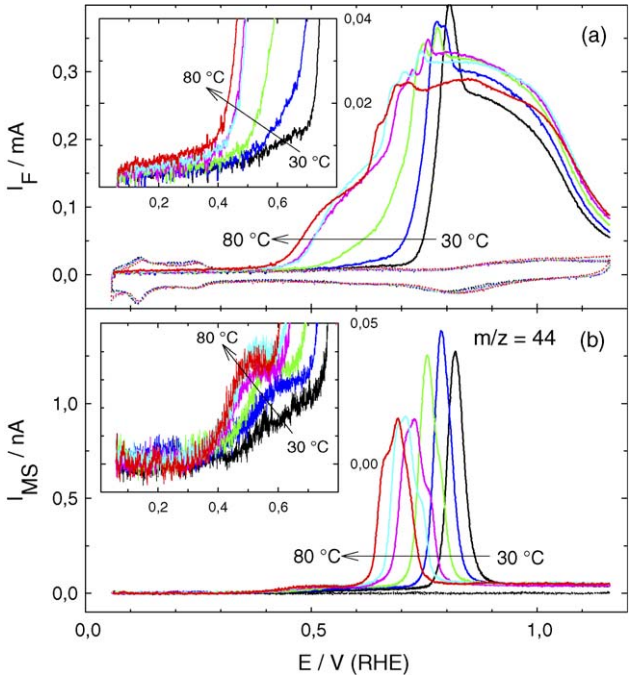

Fig. 7. Faradaic current (a) and mass spectrometric ($m/z = 44$) (b) signal for CO stripping from a CO_{ad} saturated 20 wt.% carbon-supported Pt/Vulcan catalyst electrode (7 $\mu g_{pt}\,cm^{-2}$) at different temperatures in 2%CO/H_2-saturated 0.5 M H_2SO_4 solution, after adsorption in that electrolyte for 5 min at the respective temperature (temperatures: 30, 40, 50, 60, 70, and 80 °C, scan rate 10 mV s^{-1}).

CO_{ad} saturated Pt/C catalyst electrode in 2%CO/H_2-saturated electrolyte. Under these conditions the Faradaic current signal differs significantly from the CO_2 related $m/z = 44$ signal. The major difference results from the dominant contribution of the HOR to the Faradaic current. While CO_2 formation is concentrated in a sharp main peak and proceeds only with low rates at potentials positive of the main stripping peak, H_2 oxidation occurs over a wide potential range. The reaction characteristics at 30 °C are practically identical with those reported in [21], where they are discussed in more detail.

Similar to CO_{ad} oxidation in inert electrolyte (Fig. 5), the CO_{ad} oxidation peak ($m/z = 44$) shifts to more cathodic potentials with increasing temperature. Furthermore, because of the presence of CO in the electrolyte, the main peaks are shifted to more positive potentials compared to those in Fig. 5, and the CO_{ad} coverage is practically constant up to 80 °C (Fig. 6, square symbols), in good agreement with findings in [103]. Different from CO_{ad} stripping in inert electrolyte (Fig. 5b), also the peak shape changes significantly, from a narrow peak at 30 °C to a complex multi-peak structure at higher temperatures, at 60–80 °C (Fig. 7b). In addition, for increased temperatures we find a pronounced pre-wave starting at 0.4 V. An enlarged representation of the CO_{ad} oxidation pre-wave (inset Fig. 7b) resolves that with increasing temperature a distinct peak develops in the pre-wave potential region, which starts between 0.3 and 0.4 V.

Examining the Faradaic current signal in more detail we find a continuous shift of the HOR onset potential to more cathodic values and a change of the current–potential characteristics. This is particularly obvious in the current onset in the pre-wave region, which changes from a slow increase of the H_2-oxidation current at 30 °C to an increasingly steeper onset of the HOR current at higher temperatures. The pronounced shift of the steep increase of the main Faradaic current peak (Fig. 7a) to slightly below 0.4 V at 80 °C corresponds one-to-one to the increasing pre-wave formation in CO_{ad} oxidation (Fig. 7b). Hence, these measurements clearly demonstrate that also at increasing temperatures the HOR starts with the onset of CO_{ad} oxidation (CO_2 formation). The pronounced sharp peak in the Faradaic current, which is best resolved at lower temperatures, correlates with the main peak for CO_2 formation (see also [21]). With increasing temperature this peak shifts to lower potentials and becomes less pronounced, similar to the behavior of the CO_2 peak (Fig. 7b). At potentials positive of 0.9 V_{RHE} the transport limited HOR rate decays steadily up to the positive potential limit of 1.15 V_{RHE} (Fig. 7a), which is associated with increasing Pt surface oxide formation at about constant CO_2 formation rate at potentials positive of 0.9 V [126].

The much higher Faradaic currents in the pre-wave relative to the main peak compared to the signals for CO_2 formation demonstrates the amplification effect discussed above [9], with H_2 oxidation going on in holes of the CO adlayer, which leads to considerable HOR rates even on Pt surfaces largely covered by a CO adlayer. It is important to note that the apparent contribution of this effect increases rapidly with increasing transport limitations. Hence, the situation may be very different in model experiments without enforced electrolyte transport and in an operating fuel cell with high mass transport. The results clearly demonstrate that the strong, temperature induced increase of the HOR current in the potential range of the pre-wave is mainly due the increasing contribution of pre-wave CO_{ad} oxidation and the related decrease in CO_{ad} coverage at elevated temperatures, while CO_{ad} desorption plays no role under present conditions, due to the facile CO readsorption in 2%CO/H_2-saturated electrolyte. This conclusion agrees well with our observation that there is no measurable decay in the steady-state CO_{ad} coverage up to 80 °C reaction conditions (Fig. 6, squares). If desorption would play a major role, one would expect H_2 oxidation from low potentials on.

4.1.3. Air bleed operation—removal of CO_{ad} by reaction with oxygen, and O_2 reduction on a partly CO_{ad} covered Pt/Vulcan supported catalyst

The addition of small amounts of O_2 or air (<0.5% O_2 equivalent) to the H_2-rich anode feed is a common method in order to reduce the sensitivity of low-temperature PEFCs to CO trace impurities in the anode feed by chemical reaction of the resulting CO_{ad} with adsorbed oxygen [9,127–129]. It has to be considered, however, that under anode reaction conditions O_2 reduction is possible as well, and that depending on the anode catalyst and the nature and coverage of a possible adsorbate layer this may result also in H_2O_2 formation. It had been demonstrated, for instance, that on CO_{ad} saturated polycrystalline Pt and Pt(1 1 1) electrodes O_2 reduction is still possible [8], but results largely (80% on pc-Pt, 95% on Pt/C) in H_2O_2 formation [5]. Therefore it is important to know (i) the efficiency for CO_{ad} removal by chemical oxidation, i.e., by reaction with oxygen, under anode reaction conditions, and (ii) the extent of O_2 reduction and in particular of H_2O_2 formation under these conditions on a partly CO_{ad} covered catalyst surface. These questions were topic of recent model studies on O_2 reduction and CO_{ad} oxidation during interaction of O_2 with a CO_{ad} precovered carbon-supported Pt/Vulcan catalyst electrode [6,7]. The efficiency for reactive CO_{ad} removal was investigated by reaction of a CO_{ad} saturated Pt/Vulcan catalyst electrode with 2%O_2/Ar saturated electrolyte under anode reaction conditions. The amount of CO_{ad} removal was determined by subsequent CO_{ad} stripping experiments. As illustrated in Fig. 8, the reactive CO_{ad} removal is extremely slow under these conditions. Depending on the reaction potential the CO_{ad} coverage decreases only by 3–4% at 0.06 V_{RHE} and by ~17% at 0.26 V_{RHE}, respectively, during 1 h reaction time. From the slope of the CO_{ad} coverage versus reaction time relation we can estimate that the initial reaction rate for chemical CO_{ad} oxidation, on a fully CO_{ad} saturated catalyst surface, is only 10^{-5} monolayers s^{-1} (ML s^{-1}) at 0.06 V_{RHE} and 10^{-3} (ML s^{-1}) at 0.26 V_{RHE}. These data also indicate that the reactive CO_{ad} removal ceases long before completion, which is supported also by results of similar measurements in O_2 saturated solution [7]. Apparently, it is not possible to completely remove the CO adlayer under these conditions by reaction with dissolved O_2.

The related ORR currents can be determined from the reaction transients recorded during interaction of the O_2 containing electrolyte with the CO_{ad} pre-saturated catalyst (Fig. 9). For

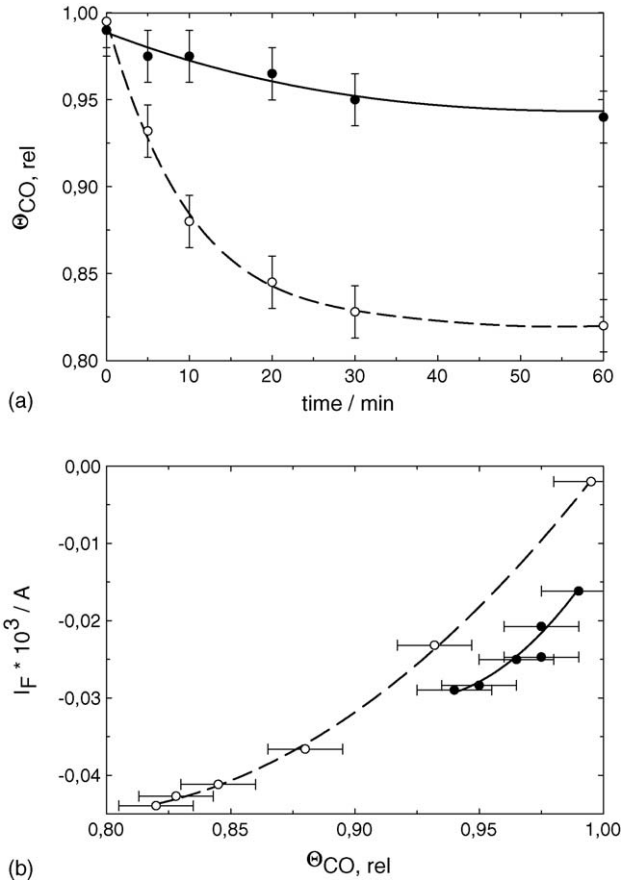

Fig. 8. Evolution of the relative CO coverages with time during the chemical oxidation of CO_{ad} on a 20 wt.% Pt/Vulcan catalyst (7 μg_{pt} cm^{-2}) with O_2 (2% O_2 in Ar) at 0.06 V_{RHE} (filled circles) and 0.26 V_{RHE} (empty circles), respectively (a) determined by integration of the CO_2 stripping signals after the experiments described in Fig. 9. (b) Relation between Faradaic current and CO_{ad} coverage as plotted in (a) (measurements for 1 h reaction time are shown in Fig. 9) (with permission from Ref. [6]).

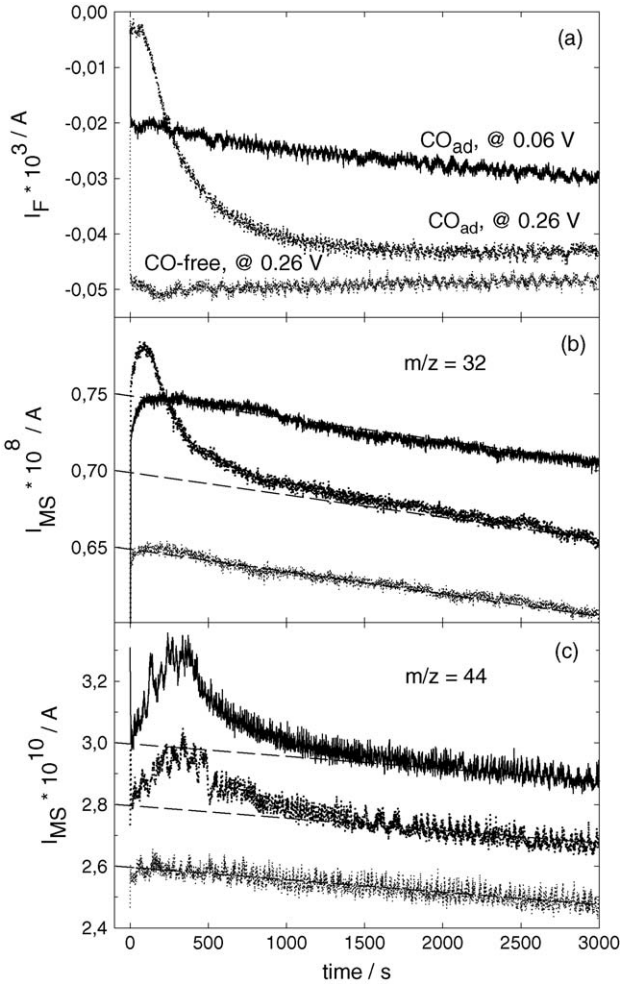

Fig. 9. Faradaic (a) and mass spectrometric current transients for $m/z = 32$ (b) and $m/z = 44$ (c) recorded during 1 h chemical CO_{ad} oxidation by reaction with a dilute O_2 atmosphere on a CO_{ad} saturated Pt/Vulcan catalysts at 0.06 V (full lines, top curves) and 0.26 V_{RHE} (dotted lines, middle curves), respectively, upon admission of a 2%O_2/Ar saturated electrolyte. For comparison the same experiment is performed on a CO_{ad} free Pt/Vulcan catalyst at 0.06 V_{RHE} (dotted lines, bottom curves). For better readability the mass spectrometric curves are offset by 0.5 nA (b) and 20 pA (c), the linear drift of the background intensity is indicated by dashed lines (with permission from Ref. [6]).

reaction at 0.06 V_{RHE} the Faradaic current transient (Fig. 9a) shows a continuous, slow increase of the (cathodic) current with time (3000 s reaction time), after an initial jump from 0 to −0.2 mA right after admission of the 2%O_2/Ar saturated electrolyte. As expected, the O_2 partial pressure (Fig. 9b) first increases steeply, followed by a slower increase during the first 100 s, until it saturates and, within the limits set by the stability of the measurement, remains at this value for the rest of the reaction time. The variation during the first 100 s is attributed to the build-up of a steady-state adlayer. The initial jump of the Faradaic current reflects the known fact that O_2 reduction is possible also on a completely CO_{ad} covered surface [5]. The subsequent increase of the (cathodic) reaction current seems to disagree with the approximately constant O_2 consumption. It can be explained, however, by a change in the contributions of the two reaction pathways, the two-electron pathway (H_2O_2 formation) and the four-electron pathway (H_2O formation). In this case H_2O_2 formation dominates at saturation coverages, but the contribution from the four-electron process increases significantly with time, i.e., with slightly decreasing CO_{ad} coverage. Based on the Faradaic current only a very small fraction of the consumed O_2, about 10^{-4}, is used for CO_{ad} oxidation, the rest is reduced to H_2O and/or H_2O_2. The transient ORR behavior on the CO_{ad} blocked Pt catalyst electrode points to a significant effect of the slowly decreasing CO adlayer coverage on the ORR characteristics.

The CO_2 partial pressure (Fig. 9c) passes through an initial maximum after about 350 s and then decays steadily, in a roughly exponential way, to its background level, which is reached after about 1500 s. Similar to the conclusions from stripping experiments the CO_2 formation rate is very low after this time. The initial signal is clear evidence of chemical CO_{ad} oxidation, by reaction with O_2, under these simulated 'air bleed' conditions. Interestingly, we found the charge in the initial CO_2 peak to be consistently higher than the CO_{ad} loss derived from the subsequent stripping measurements, which was tentatively explained by oxidation of small amounts of the Vulcan support material, e.g., at defects [6].

At 0.26 V_{RHE} reaction potential the reaction induced changes are more pronounced and faster, as expected from the results in Fig. 8. But even under these conditions the mass transport limited ORR current (Fig. 9a) and O_2 consumption (Fig. 9b) are not fully reached during 1 h reaction time, as shown by comparison with O_2 reduction on a CO_{ad} free Pt catalyst electrode (Fig. 9a and b). On the other hand, the initial O_2 reduction rate and O_2 consumption on the CO_{ad} saturated surface are much lower than at 0.06 V_{RHE} reaction potential, in agreement with the results of potentiodynamic measurements on a CO_{ad} covered Pt catalyst [6].

Finally, the extent of H_2O_2 formation under similar reaction conditions was followed by flow cell measurements in a double-disk electrode dual thin-layer flow cell [7], where H_2O_2 formation at the working electrode ('generator') is detected by oxidation at a second electrode ('collector') which is held at anodic potential [27] (Fig. 10). The Faradaic current transient (Fig. 10a) closely resembles that in Fig. 9a, considering that in this case the electrolyte was saturated with pure O_2 rather than with a 2%O_2/Ar mixture. But also for the much higher O_2 concentration it does not reach the mass transport limited current during the reaction time (480 s), which is indicated again by the ORR current obtained on a CO_{ad} free Pt catalyst. The collector current depicted in Fig. 10b shows significant H_2O_2 formation at the beginning of the reaction, after admission of the O_2 saturated electrolyte. The H_2O_2 yield calculated from the collector current, which is shown in Fig. 10c, starts from values of around 90% and then decays exponentially to about 30%. At this point about 20% of the CO adlayer are removed. It is interesting to note that the collector current and hence the H_2O_2 formation is significantly higher on a CO_{ad} blocked Pt catalyst electrode than on a Pt-free Vulcan electrode. On the other hand, it is significantly lower on the CO_{ad} free Pt catalyst electrode than on the Pt-free Vulcan electrode, indicating that part of the H_2O_2 formed on the carbon support material is fully oxidized on the Pt nanoparticles [6].

Finally, the potential dependence of the O_2 consumption at different CO_{ad} coverages was investigated in potentiodynamic DEMS measurements, where we followed the Faradaic current, the CO_2 ion current ($m/z = 44$) and the O_2 ion current ($m/z = 32$) during CO_{ad} stripping in 2%O_2/Ar saturated electrolyte after different times of CO_{ad} oxidation in this solution at 0.06 V (related reaction transients see Fig. 9). These data, which are shown and discussed in more detail in Ref. [6], demonstrate that on a fully CO_{ad} saturated Pt/Vulcan catalyst O_2 reduction occurs only at the most cathodic potentials, below 0.3 V. With slightly decreasing CO_{ad} coverage – a coverage reduction on the order of a few percent is sufficient – O_2 consumption and O_2 reduction occur over the entire potential regime typical for the ORR on Pt, i.e., up to 0.8–0.9 V. Hence, under present transport conditions very small reductions in CO_{ad} coverage are sufficient to fully consume the transport limited O_2 supply at potentials below 0.8 V.

Similar observations of an increased H_2O_2 formation of up to 100% and of very slow CO_{ad} removal were reported also in a very recent RRDE study on the same reaction on a CO_{ad} precovered single crystal Pt(1 1 1) electrodes [8], and led the authors to similar conclusions.

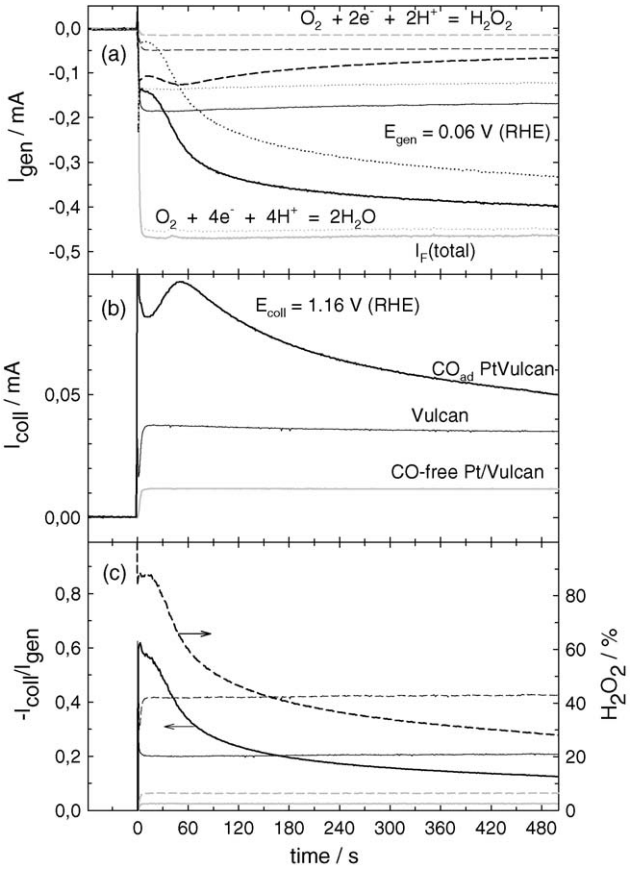

Fig. 10. Simultaneously recorded current transients after starting to flow O_2-saturated electrolyte over a CO_{ad} blocked Pt/Vulcan catalyst (black thick lines), CO_{ad} free Pt/Vulcan catalyst (gray lines) (Pt loading 28 μg cm^{-2}) or Pt-free Vulcan carbon support (black thin lines) at 0.06 V. (a) Faradaic current transients on the working electrode in the first compartment and (b) H_2O_2 oxidation currents on poly crystalline Pt (collector, $E = 1.16$ V) in the second compartment of the dual thin-layer flow cell; (c) corresponding hydrogen peroxide yields. Electrolyte flow rate ca. 4 μl s^{-1}, room temperature, assignment of the lines: dashed lines (a): partial current for oxygen reduction to hydrogen peroxide calculated according to Eq. (1) in Ref. [7], dotted lines (a): partial current for oxygen reduction to water calculated as the difference between the net current and partial hydrogen peroxide formation current, full lines (a): total Faradaic current on the working electrode; full line (c): H_2O_2 current yield (left), dashed line (c): H_2O_2 yield (right) (with permission from Ref. [7]).

These findings have important implications for technical air bleed applications. They clearly demonstrate that air bleed operation may lead to significant H_2O_2 formation, which is less problematic from the point of the efficiency of the fuel cell, but would have disastrous consequences for the stability of the membrane. Furthermore, they imply that air bleed operation should be performed in such a way that higher CO_{ad} coverages are avoided, since H_2O_2 formation increases steeply under these conditions [7]. Hence, air bleed operation is not a suitable option for using fuel gases with CO contaminations much above the levels commonly acceptable for PtRu catalyst electrodes, since at reaction probabilities between 10^{-4} and 10^{-5} the O_2 contents required and hence also the H_2O_2 formation would reach intolerable levels in that case [7]. Considering the catalyst and membrane stability problems associated with H_2O_2 formation, we rather question whether continuous O_2 additions

significant above the O_2 level in the anode due to O_2 permeation from the cathode [101] makes sense at all, or whether this should be limited to short-term additions, e.g., in response to CO spikes in the reformate based feed gas during dynamic operation. As an alternative the oxidative removal of adsorbed CO at the anode by short-term electrochemical pulsing was proposed [130].

Finally it is interesting to compare these results with the situation typical for the catalytic CO removal from CO contaminated feed gases by preferential CO oxidation (PROX) (see, e.g., [131] and references therein). For reaction on a supported Pt catalyst typically 20–50% of the O_2 is consumed for CO oxidation, the remaining fraction reacts with H_2 in the feed gas [131]. Hence the selectivity for CO oxidation is much higher under PROX conditions, where O_2 reduction is excluded, than during air bleed fuel cell anode operation. It should be noted, however, that the simulated air bleed model studies did not include H_2 in the feed gas; studies using more realistic feed gas mixtures and at elevated temperatures are still missing. Although it appears likely that chemical oxidation of H_2 is much slower than the very fast electrooxidation of H_{ad} to H^+, it is hard to predict how the former rate will compare to the rate for chemical CO_{ad} oxidation, considering the very low probability for the latter reaction.

4.2. CO_2 adsorption/reduction and H_2 oxidation in CO_2/H_2 mixtures on Pt/Vulcan and PtRu/Vulcan supported catalyst

Reformate gases generally contain significant amounts of CO_2, e.g., around 20% in reformate generated by natural gas reforming and subsequent catalytic CO removal. In view of this considerable amount of CO_2 questions about the effect of CO_2 on the HOR are obvious, in particular when comparing it with the dramatic influence of the much smaller CO concentrations. Under anode reaction conditions (potentials) one would expect some CO_2 reduction to occur, with CO as one of the possible reaction products. Since at the desired anode reaction conditions CO_{ad} electrooxidation is not possible on Pt, the anode catalyst should be slowly poisoned by a CO adlayer. Interestingly, fuel cell measurements using CO_2 rich reformate as feed gas found only small CO_2 induced effects on the current density and reaction behavior of the fuel cell, less than those imposed by CO even at ppm levels [115,129,132–134]. Depending on the preparation and structure of the Pt/Vulcan electrode the cell performance was found to deteriorate by up to 30% when the anode is fed with 20% CO_2 in H_2 at a cell potential of 0.5 V_{RHE} [133]. Previous model studies focused on the nature of the adsorbed species resulting from CO_2 adsorption at various potentials, which was investigated by various techniques (for an overview see Ref. [75]). The influence of CO_2 on the electrooxidation of H_2 has not been investigated in model studies so far.

Comparative chronoamperometric and mass spectrometric DEMS measurements following the Faradaic current and the H_2 partial pressure upon reaction of pure H_2 and of a 20%CO_2/H_2 mixture on a carbon-supported Pt/Vulcan catalyst electrode ($E = 0.06$ V_{RHE}) indeed show stable signals in both cases over 1500 s, and the absolute values differ by about the reduction in H_2 partial pressure [75]. Apparently, under present reaction conditions the effect of the CO_2 is even less than in the fuel cell measurements described above, reflecting just the reduction in H_2 partial pressure. On the other hand, stripping experiments performed after 25 min reaction of the Pt/Vulcan electrode in 0.5 M H_2SO_4 solution purged with a 20%CO_2/H_2 mixture show significant build-up of an adsorbate layer, which based on the oxidation charge is identified as CO_{ad}. This assignment is confirmed also by in situ SEIRAS measurements on Pt thin film electrodes during reaction with 20%CO_2/H_2, which show distinct C–O stretch vibrations at 1900–1700 and 2100–2000 cm^{-1} (depending on the CO_{ad} coverage) in linearly (CO_L) and multiply (CO_M) bonded configurations, respectively, as only additional signals upon interaction of CO_2 with the Pt electrode (for further details see Ref. [75]). Interestingly, the resulting CO_{ad} saturation coverages are significantly lower than those obtained by CO adsorption, reaching ca. 50% of the CO_{ad} saturation coverage in 20%CO_2/Ar mixtures and ~60% in 20%CO_2/H_2 mixtures (see Fig. 11). The resulting CO_{ad} coverage depends strongly on the reaction potential, and decays rapidly from the above values at potentials positive of 0.15 V_{RHE}. At potentials positive of 0.3 V_{RHE} CO_{ad} formation via reductive adsorption of CO_2 is practically inhibited.

From these findings we concluded that CO_2 reduction on the Pt/Vulcan catalyst is much more sensitive to the presence of a CO submonolayer than the HOR. CO_2 reduction ceases at CO_{ad} coverages of ca. 50% of the CO_{ad} saturation coverage obtained by adsorption from CO-saturated electrolyte. At these CO_{ad} coverages the HOR still proceeds with significant rates (Figs. 1 and 2). This behavior closely resembles that of dissociative methanol or ethanol adsorption, which equally stops at CO_{ad} coverages well below the saturation coverage and where similar effects were made responsible [20,30]. Different from the latter cases, however, CO_2 reduction is not inhibited by the H-upd adlayer largely covering the surface at very cathodic potentials, but proceeds only in the potential range where H-upd is still present ($\leq$0.3 V_{RHE}). This observation indicates that CO_2 reduction proceeds via reaction with coadsorbed H_{ad}. Further details on the

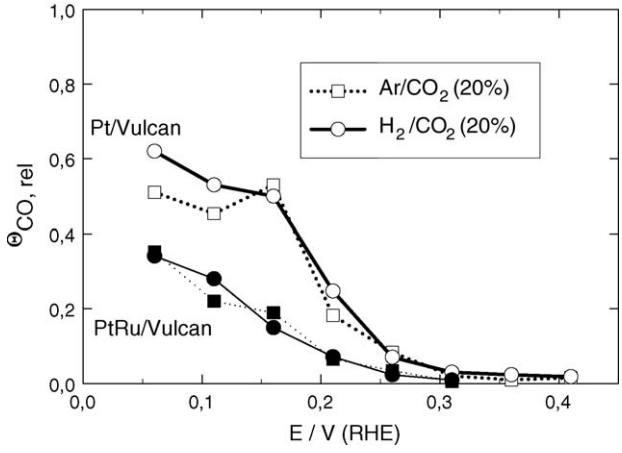

Fig. 11. Relative CO_{ad} coverage after 25 min CO_2 reduction on a 20 wt.% Pt/Vulcan electrode (empty symbols) and on a 20 wt.% PtRu/Vulcan electrode (filled symbols (loading 28 ng_{metal} cm^{-2}) in 0.5 M H_2SO_4 solution saturated with Ar/CO_2(20%) (circles) and H_2/CO_2(20%) (squares) gas mixtures as a function of adsorption potential (adsorption time 25 min, room temperature).

CO_2 reduction on Pt thin films and Pt/Vulcan electrodes can be found in Ref. [75].

Similar observations were reported also from measurements in a laboratory-type single cell set-up using a realistic Pt/Vulcan based membrane electrode assembly (MEA), both at room temperature and at 60 °C, indicating that the mechanistic explanation derived from our model studies holds true also under fully realistic fuel cell reaction conditions [75]. Following our above discussion we suggest that the influence of the CO adlayer and hence also of CO_2 contaminations will depend sensitively on the transport conditions and catalyst loading. Under HOR reaction conditions, which are purely controlled by the reaction kinetics and not by mass transport effects, we would expect more pronounced effects (see also the discussion in Section 4.1.1).

The effect of the nature of the catalyst becomes evident by comparing the CO_{ad} coverages resulting from interaction of Pt/Vulcan and PtRu/Vulcan electrodes with 20%CO_2/Ar and 20%CO_2/H_2 mixtures. The CO_{ad} coverages obtained on the PtRu/Vulcan electrode are included as filled symbols in Fig. 11. In this case the reductive CO_2 adsorption and hence CO_{ad} formation stops at even lower coverages than on Pt/Vulcan. This can be explained by two different effects, either by (i) the weaker CO_{ad} adsorption on PtRu compared to Pt [135], which could shift the effective barrier for CO_2 reduction to higher values compared to Pt (Bronstedt–Evans–Polanyi relation [136]), and/or by (ii) a less dense and less strongly bound H-upd adlayer on the alloy [135], which can inhibit the further reaction with CO_2 at lower CO_{ad} coverages, due to H_{ad} displacement by CO_{ad}.

4.3. Model studies on long-term catalyst deactivation

Finally, as a first attempt for model studies on the long-term deactivation of anode and cathode catalysts, we studied the deactivation of Pt/Vulcan supported catalyst electrodes under anodic or cathodic reaction conditions, in H_2 or O_2 saturated electrolyte and at relevant potentials, respectively, in a wall-jet configuration, circulating about 300 ml of electrolyte driven by a piston pump [137,138].

Poisoning of a polycrystalline Pt electrode under anodic reaction conditions (room temperature, 0.16 V_{RHE}) is illustrated in Fig. 12. In H_2-saturated electrolyte the HOR rate decays linearly, loosing about 20% of its initial activity per hour. After about 3 h reaction time the current versus time curve bends of and the further current decay occurs about exponentially. After 25 h reaction time the remaining current is below the resolution of this scale.

These measurements clearly demonstrate that even after meticulous cleaning procedures and using high purity gases and chemicals as well as ultrapure water anode poisoning proceeds on a time-scale of a few hours for reaction at room temperature and at 1 ml s^{-1} electrolyte flow. The Pt electrode acts as a scavenger for trace contaminants present in the electrolyte, which even under optimal conditions are sufficient for completely covering the active Pt surface. For instance, for a total electrolyte volume of 0.25 l, an estimated concentration of 10^{-7} mol l^{-1} of active contaminants, an active Pt surface of 0.28 cm^2 and a saturation concentration of 10^{15} molecules cm^{-2} the total amount

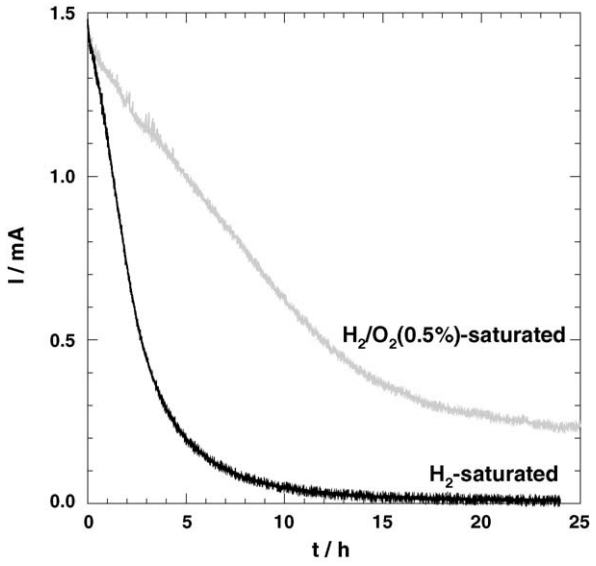

Fig. 12. Wall-jet long-term current transient measurements of the HOR on a polycrystalline Pt electrode (0.28 cm^2 surface area, 1 ml s^{-1}, 0.16 V_{RHE}) in H_2-saturated and 0.5%O_2/H_2-saturated 0.5 M H_2SO_4 solution.

of poisoning contaminants present in the electrolyte would be equivalent to a coverage of about 24 monolayers on the active Pt surface. Even larger amounts of contaminants can be dissolved into the electrolyte during a long-term model experiment from the periphery of the set-up such as glassware and tubing, especially the pump head, which are in contact with the electrolyte over a long time period, or be introduced via the feed gas.

Adding 0.5% O_2 to the H_2 feed gas results in a very different behavior (Fig. 13): While the characteristic decay down to 40% of the initial current value occurs also under these conditions, the decay is much slower and requires about 13 h. After this initial decay, the further loss of HOR current is much smaller than in the first experiment, resulting in a stable steady-state current of about 0.2 mA, which is about 15% of the initial value. Obviously, small amounts of O_2 in the feed gas seem to be able to

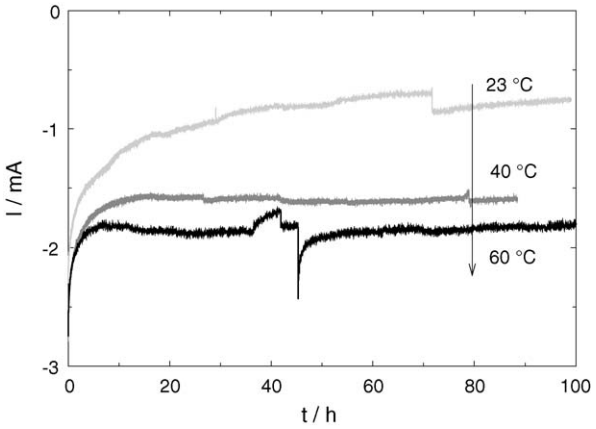

Fig. 13. Wall-jet long-term current transient measurements of the ORR on a carbon-supported 20 wt.% Pt/Vulcan catalyst electrode (loading 7 μg_{metal} cm^{-2}, 0.5 V_{RHE}) in O_2-saturated 0.5 M H_2SO_4 solution at different temperatures (20, 40, and 60 °C).

oxidatively remove part of the adsorbed contaminants. However, similar to the situation during air bleed operation only a very small fraction of the O_2 interacting with the surface will be used for the chemical oxidation of these species, the dominant fraction of the reacting O_2 will be reduced to H_2O and possibly also to H_2O_2. The presence of accumulated H_2O_2 in the electrolyte after the long-term experiments was actually detected by subsequent voltammetric measurements. As shown in [6,7], the latter reaction path will become increasingly important at high coverages of poisoning species, but is negligible at lower coverages. The low selectivity for the chemical oxidation of poisoning species can be illustrated by a simple calculation: Under present reaction conditions the transport limited ORR current is about 2.5 mA (see Fig. 13). Assuming that (i) it needs about 1 O_2 molecule per oxidation of 1 adsorbed poisoning species, where these species may result from dissociative adsorption of larger molecules, (ii) a maximum, saturation coverage of 10^{15} adsorbed species per square centimeter, (iii) an active surface area of 0.28 cm^2, and (iv) as an admittedly crude model, that the decrease in HOR current is linearly related to the coverage of poisoning species, we can estimate a consumption of 10^{10} O_2 molecules s^{-1} for the oxidation of these species. On the other hand, the transport limited ORR current on this electrode in O_2 saturated electrolyte was found to be 2.5 mA (see Fig. 13). Hence, in 0.5%O_2/H_2-saturated electrolyte we can estimate an ORR current of 12.5 μA, corresponding to 2×10^{13} O_2 molecules s^{-1}. This means that less than 1‰ of the reacting oxygen takes part in the oxidation of poisoning adsorbates, while the majority of the reacting O_2 will be reduced (selectivity for poison oxidation <0.001). This conclusion resembles our findings for air bleed operation, where equally only a very small fraction of the reacting oxygen was involved in CO_{ad} oxidation, while the majority was reduced to H_2O and H_2O_2.

Current transients following the oxygen reduction reaction (ORR) on a carbon-supported Pt/Vulcan catalyst electrode at a constant potential of 0.5 V and similar electrolyte flow, but at different reaction temperatures of 20, 40 and 60 °C, respectively, are plotted in Fig. 13. Starting from a transport limited current of about 2.5 mA the current decays rapidly during the first few hours and then slowly approaches its steady-state value. For the lowest temperature this second phase takes almost the entire time of the measurement (100 h), with increasing temperature it becomes shorter, at 60 °C steady-state conditions are reached already after less than 10 h. The value of the final current reached under steady-state conditions increases with temperature, by more than a factor of two from 20 to 60 °C. The increase of the transport limited ORR current with temperature results from a combination of different effects: (i) the higher O_2 diffusivity at elevated temperatures, (ii) a counteracting decrease in O_2 solubility, (iii) a chemical activation of the chemical oxidation of poisoning adsorbates.

It should be noted that in addition to these chemical effects, subsequent TEM analysis showed agglomeration and/or loss of catalyst particles after our long-term wall-jet measurements, which will equally contribute to the loss of active surface. These effects are at least equally important for the understanding are of deactivation processes, but out of the scope of the present paper.

The results presented above lead to interesting consequences for the understanding of PEFC operation, which shall be discussed briefly. According to the above results already minute contaminant concentrations should suffice in order to eventually poison the anode in an operating fuel cell. This is particularly true when considering that the contamination level in an operating fuel cell, which results from electrode materials, from the feed gas and from other fuel cell components, will certainly be higher than that achieved under 'clean' conditions, on a pure Pt electrode. This should still hold true even if we consider the much larger amount of active catalyst and the generally much lower catalyst utilization in a fuel cell MEA. The latter effects may affect the time required for poisoning, but not the final result of complete poisoning, as long as the poison removal rate is practically zero. Therefore it is interesting to speculate why this is not the case. First of all operation at elevated temperatures is expected to reduce the rate and extent also of anode catalyst poisoning, similar to the observations for cathode poisoning. Second, we suggest that O_2 cross-over from the cathode compartment plays a vital role in removing oxidizable contaminants by chemical reaction with oxygen under anode reaction conditions, which can be considered as a kind of 'internal air bleed' (see also [101]). O_2 permeation through standard polymer membranes is known to occur at diffusion rates on the order of 10^{-5} cm^2 s^{-1} [94]. Further experiments to substantiate this latter idea are in progress.

5. Conclusions

Based on model studies performed mainly on carbon-supported Pt/Vulcan catalyst electrodes under fuel cell relevant conditions we have demonstrated the potential of such model studies for the understanding of fuel cell typical electrocatalytic reactions in general and specifically for catalyst poisoning and temperature effects. The importance of fuel cell relevant reactions and mass transport conditions as well as relevant catalyst materials has been demonstrated in different examples. In model studies of H_2 or reformate operated PEFCs mass transport is particularly important because of the low reactant concentrations, which are in the millimolar range. The important role of elevated temperatures was illustrated for CO adsorption and H_2 oxidation in the presence of CO in the feed gas, which shows a drastic decay of the onset potential of the HOR with increasing temperature. Based on these data this shift is caused by the shift of the onset for CO oxidation rather than by a lower steady-state CO_{ad} coverage due to thermal desorption. The astonishingly low effect of CO_2 in the feed gas, which is present at levels 20% and more in feed gases generated by reforming of low-C hydrocarbons, could be shown to be due to the inhibition of CO_2 reduction to CO_{ad} at CO_{ad} submonolayer coverages which are too low to significantly affect the H_2 oxidation rate. Model studies on the long-term stability of Pt anode catalysts in pure H_2 and in 0.5%O_2/H_2-saturated electrolyte as well as on the effect of air bleed operation in CO contaminated feed gas show an extremely low selectivity for adsorbate oxidation of below 1‰. Most of the O_2 reacting at the anode is reduced to H_2O or, on surfaces with high adsorbate coverages, to H_2O_2, which may have significant implications on

the stability of the membrane and the carbon support. They also demonstrate that under anode reaction conditions, where electrooxidation of adsorbed impurities is impossible, complete poisoning is reached after few hours in the absence of O_2 in the feed gas, indicating that O_2 permeation from the cathode to the anode compartment is important for the stability of fuel cell operation.

Acknowledgements

We gratefully acknowledge the contributions of H.A. Gasteiger, T.J. Schmidt, U.A. Paulus, J. Kaiser, Y.X. Chen, H. Wang, M. Heinen, L. Colmenares, and E. Guerrini in the course of this work, and the good collaboration with the Center of Solar Energy and Hydrogen Research (ZSW Ulm) and with the group of Prof. H. Bönnemann (MPI for Coal Research, Mülheim). Financial support for this work came from the Federal Ministry of Education and Research (BMBF), the Deutsche Forschungsgemeinschaft (Be 1201/8, Be 1201/11), the Ministry of Science, Research and the Arts of the State of Baden-Württemberg und the Research Alliance Fuel Cells, Baden, Württemberg.

References

[1] J.S. Wainright, M.H. Litt, R.F. Savinell, in: W. Vielstich, H.A. Gasteiger, A. Lamm (Eds.), Handbook of Fuel Cells—Fundamentals, Technology and Applications, vol. 3, Wiley & Sons, Chichester, 2003.
[2] Q. Li, R. He, J.-A. Gao, J.O. Jensen, N.J. Bjerrum, J. Electrochem. Soc. 150 (2003) A1599.
[3] A.P. Saab, F.H. Garzon, T.A. Zawodzinski, J. Electrochem. Soc. 150 (2003) A214.
[4] Y.-L. Ma, J.S. Wainright, M.H. Litt, R.F. Savinell, J. Electrochem. Soc. 151 (2004) A8.
[5] N.M. Markovic, T.J. Schmidt, V. Stamenkovic, P.N. Ross, Fuel Cells 1 (2001) 105.
[6] Z. Jusys, J. Kaiser, R.J. Behm, J. Electroanal. Chem. 554–555 (2003) 427.
[7] Z. Jusys, R.J. Behm, J. Phys. Chem. B 108 (2004) 7893.
[8] V. Stamenkovic, B.N. Grgur, P.N. Ross, N.M. Markovic, J. Electrochem. Soc. 152 (2005) A277.
[9] S. Gottesfeld, J. Pafford, J. Electrochem. Soc. 135 (1988) 2651.
[10] T.J. Schmidt, H.A. Gasteiger, G.D. Stäb, P.M. Urban, D.M. Kolb, R.J. Behm, J. Electrochem. Soc. 145 (1998) 2354.
[11] T.J. Schmidt, M. Noeske, H.A. Gasteiger, R.J. Behm, P. Britz, W. Brijoux, H. Bönnemann, J. Electrochem. Soc. 145 (1998) 925.
[12] T.J. Schmidt, H.A. Gasteiger, R.J. Behm, J. Electrochem. Soc. 146 (1999) 1296.
[13] T.J. Schmidt, H.A. Gasteiger, R.J. Behm, Electrochem. Commun. 1 (1999) 1.
[14] T.J. Schmidt, H.A. Gasteiger, R.J. Behm, J. New Mater. Electrochem. Syst. 2 (1999) 27.
[15] T.J. Schmidt, U.A. Paulus, H.A. Gasteiger, N. Alonso-Vante, R.J. Behm, J. Electrochem. Soc. 147 (2000) 2620.
[16] U.A. Paulus, U. Endruschat, G.J. Feldmeyer, T.J. Schmidt, H. Bönnemann, R.J. Behm, J. Catal. 195 (2000) 383.
[17] U.A. Paulus, T.J. Schmidt, H.A. Gasteiger, R.J. Behm, J. Electrochem. Soc. 495 (2001) 134.
[18] J. Kaiser, Z. Jusys, R.J. Behm, R. Mörtel, H. Bönnemann, in: F.N. Büchi, G.G. Scherer, A. Wokaun (Eds.), Proceedings of the First European Fuel Cell Forum, European Fuel Cell Forum, Luzern, 2001, pp. 59–62.
[19] T.J. Schmidt, Z. Jusys, H.A. Gasteiger, R.J. Behm, U. Endruschat, H. Bönnemann, J. Electroanal. Chem. 501 (2001) 132.
[20] Z. Jusys, R.J. Behm, J. Phys. Chem. B 105 (2001) 10874.
[21] Z. Jusys, J. Kaiser, R.J. Behm, Phys. Chem. Chem. Phys. 3 (2001) 4650.
[22] J. Kaiser, L. Colmenares, Z. Jusys, R. Mörtel, H. Bönnemann, G. Köhl, H. Modrow, J. Hormes, R.J. Behm, submitted for publication.
[23] Z. Jusys, J. Kaiser, R.J. Behm, Electrochim. Acta 47 (2002) 3693.
[24] Z. Jusys, T.J. Schmidt, L. Dubau, K. Lasch, L. Jörissen, J. Garche, R.J. Behm, J. Power Sources 105 (2002) 297.
[25] U.A. Paulus, T.J. Schmidt, H.A. Gasteiger, in: W. Vielstich, H.A. Gasteiger, A. Lamm (Eds.), Handbook of Fuel Cells—Fundamentals, Technology, Applications, vol. 2, Wiley & Sons, Chichester, 2003.
[26] Z. Jusys, J. Kaiser, R.J. Behm, Langmuir 19 (2003) 6759.
[27] Z. Jusys, J. Kaiser, R.J. Behm, Electrochim. Acta 49 (2004) 1297.
[28] Z. Jusys, R.J. Behm, submitted for publication.
[29] H. Wang, Z. Jusys, R.J. Behm, J. Power Sources, in press.
[30] H. Wang, Z. Jusys, R.J. Behm, Fuel Cells 4 (2004) 113.
[31] H. Wang, Z. Jusys, R.J. Behm, J. Phys. Chem. B 108 (2004).
[32] H. Wang, Z. Jusys, R.J. Behm, submitted for publication.
[33] H. Wang, Z. Zhao, Z. Jusys, R.J. Behm, J. Power Sources, in press.
[34] Y.-X. Chen, M. Heinen, Z. Jusys, R.J. Behm, submitted for publication.
[35] Y.-X. Chen, S. Ye, M. Osawa, Z. Jusys, R.J. Behm, submitted for publication.
[36] Z. Jusys, R.J. Behm, Electrochim. Acta 49 (2004) 3891.
[37] H. Gerischer, I. Mattes, R. Braun, J. Electroanal. Chem. 10 (1965) 553.
[38] W.J. Albery, C.C. Jones, A.R. Mount, in: R.G. Compton, A. Hamnett (Eds.), Chemical Kinetics, vol. 29, Elsevier Publ., Amsterdam, Oxford, New York, Tokyo, 1986.
[39] C.M.A. Brett, A.M.F.C. Oliveira Brett, in: C.H. Bamford, R.G. Compton (Eds.), Chemical Kinetics, vol. 26, Elsevier Publ., Amsterdam, Oxford, New York, Tokyo, 1986.
[40] T.H. Madden, N. Arvindan, E.M. Stuve, J. Electrochem. Soc. 150 (2003) E1–E10.
[41] J. Yamada, H. Matsuda, J. Electroanal. Chem. 44 (1973) 189.
[42] W.J. Albery, J. Electroanal. Chem. 191 (1985) 1.
[43] M. Bergelin, M. Wasberg, J. Electroanal. Chem. 449 (1998) 181.
[44] M. Bergelin, E. Herrero, J.M. Feliu, M. Wasberg, J. Electroanal. Chem. 467 (1999) 74.
[45] A.N. Frumkin, L. Nekrasov, V.G. Levich, J. Ivanov, J. Electroanal. Chem. 1 (1959) 84.
[46] V.G. Levich, Physicochemical Hydrodynamics, Prentice-Hall, Eaglewood Cliffs, NJ, 1962.
[47] N.M. Markovic, P.N. Ross Jr., Surf. Sci. Rep. 45 (2002) 117.
[48] N. Wakabayash, M. Takeichi, M. Itagaki, H. Uchida, M. Watanabe, J. Electroanal. Chem. 574 (2005) 339.
[49] F. Gloaguen, F. Andolfatto, R. Durand, P. Ozil, J. Appl. Electrochem. 24 (1994) 863.
[50] S.L. Gojkovic, S.K. Zesevic, R.F. Savinell, J. Electrochem. Soc. 145 (1998) 3713.
[51] F. Gloaguen, P. Convert, S. Gamburzev, O.A. Velev, S. Srinivasan, Electrochim. Acta 43 (1998) 3767.
[52] K.W. Feindel, L.P.A. LaRocque, D. Starke, S.H. Bergens, R.E. Wasyleshen, J. Am. Chem. Soc. 126 (2004) 11436.
[53] T. Iwasita, X. Xia, E. Herrero, H.-D. Liess, Langmuir 12 (1996) 4260.
[54] T. Toda, H. Igarashi, H. Uchida, M. Watanabe, J. Electrochem. Soc. 146 (1999) 3750.
[55] N.M. Markovic, C.A. Lucas, A. Rodes, V. Stamenkovic, P.N. Ross, Surf. Sci. 499 (2002) L149.
[56] U.A. Paulus, A. Wokaun, G.G. Scherer, T.J. Schmidt, V. Stamenkovic, V. Radmilovic, N.M. Markovic, P.N. Ross Jr., J. Phys. Chem. B 106 (2002) 4181.
[57] T. Iwasita-Vielstich, in: H. Gerischer, C.W. Tobias (Eds.), Advances in Electrochemical Science and Engineering, VCH Verlagsgesellschaft, Weinheim, 1990.
[58] B. Bittins-Cattaneo, E. Cattaneo, P. Königshoven, W. Vielstich, in: A.J. Bard (Ed.), Electroanalytical Chemistry. A Series of Advances, vol. 17, Marcel Dekker, New York, 1991, p. 181.
[59] S.-G. Sun, in: J. Lipkowski, P.N. Ross (Eds.), Electrocatalysis, Wiley–VCH, New York, 1998.

[60] H. Baltruschat, in: A. Wieckowski (Ed.), Interfacial Electrochemistry—Theory, Experiment and Applications, Marcel Dekker Inc., New York, 1999.
[61] P.A. Christensen, in: A.J. Bard, M. Stratmann, P.R. Unwin (Eds.), Instrumentation and Electroanalytical Chemistry, vol. 3, Wiley–VCH, Chichester, 2003.
[62] T. Iwasita, F.C. Nart, Prog. Surf. Sci. 55 (1997) 271.
[63] M. Osawa, K. Ataka, K. Yoshi, T. Yotsuyanagi, J. Electron Spectrosc. Rel. Phenom. 64–65 (1993) 371.
[64] M. Osawa, Handbook of Vibrational Spectroscopy, Wiley–VCH, Chichester, 2002.
[65] A. Miki, S. Ye, M. Osawa, Chem. Commun. (2002) 1500.
[66] Y.-X. Chen, A. Miki, S. Ye, H. Sakai, M. Osawa, J. Am. Chem. Soc. 125 (2003) 3680.
[67] A. Miki, S. Ye, T. Sensaki, M. Osawa, J. Electroanal. Chem. 563 (2004) 23.
[68] Y.-X. Chen, M. Heinen, Z. Jusys, R.J. Behm, Angew. Chem., in press.
[69] K.A. Friedrich, F. Henglein, U. Stimming, W. Unkauf, Electrochim. Acta 47 (2001) 689.
[70] V. Stamenkovic, M. Arenz, P.N. Ross, N.M. Markovic, J. Phys. Chem. B 1108 (2004) 17915.
[71] C. Rice, Y.Y. Tong, E. Oldfield, A. Wieckowski, F. Hahn, F. Gloaguen, J.M. Leger, C. Lamy, J. Phys. Chem. B 104 (2000) 5803.
[72] W. Chen, S.-G. Sun, Z.-Y. Zhou, S.-P. Chen, J. Phys. Chem. B 107 (2003) 9808.
[73] F. Maillard, E.R. Savinova, P.A. Simonov, V.I. Zaikovskii, U. Stimming, J. Phys. Chem. B 108 (2004) 17893.
[74] O. Wolter, J. Heitbaum, Ber. Bunsenges. Phys. Chem. 88 (1984) 2.
[75] T. Smolinka, M. Heinen, Y.-X. Chen, Z. Jusys, W. Lehnert, R.J. Behm, Electrochim. Acta, Electrochim. Acta 50 (2005) 5189.
[76] Z. Jusys, H. Massong, H. Baltruschat, J. Electrochem. Soc. 146 (1999) 1093.
[77] Z. Jusys, J. Kaiser, R.J. Behm, in: F.N. Büchi, G.G. Scherer, A. Wokaun (Eds.), Proceeding of the First European Fuel Cell Forum, European Fuel Cell Forum, Luzern, 2001, pp. 73–78.
[78] H. Wang, Ch. Wingender, H. Baltruschat, M. Lopez, M.T. Reetz, J. Electroanal. Chem. 509 (2001) 163.
[79] Q. Fan, C. Pu, K.L. Ley, E.S. Smotkin, J. Electrochem. Soc. 143 (2006) L21–L23.
[80] I. Tkach, A. Panchenko, T. Kaz, V. Gogel, K.A. Friedrich, E. Roduner, Phys. Chem. Chem. Phys. 6 (2004) 5419.
[81] S. Wasmus, J.-T. Wang, R.F. Savinell, J. Electrochem. Soc. 142 (1995) 3825.
[82] J.-T. Wang, S. Wasmus, R.F. Savinell, J. Electrochem. Soc. 143 (1996) 1233.
[83] M. Weber, J.-T. Wang, S. Wasmus, R.F. Savinell, J. Electrochem. Soc. 143 (1996) L158.
[84] V.M. Schmidt, R. Ianniello, H.-F. Oetjen, H. Reger, U. Stimming, in: S. Gottesfeld, G. Halpert, A.R. Landgrebe (Eds.), Proceedings of the First International Symposium on Proton Conducting Membrane Fuel Cells I, ECS Conference Proceeding 95–23, The Electrochemical Society, Pennington, NJ, 1995, p. 267.
[85] T. Seiler, E.R. Savinova, K.A. Friedrich, U. Stimming, Electrochim. Acta 49 (2004) 3927.
[86] N.M. Markovic, in: W. Vielstich, H.A. Gasteiger, A. Lamm (Eds.), Handbook of Fuel Cells—Fundamentals, Technology and Applications, vol. 2, Wiley & Sons, Chichester, 2003.
[87] S. Gottesfeld, T.A. Zawodzinski, in: R.C. Alkire, H. Gerischer, D.M. Kolb, C.W. Tobias (Eds.), Advances in Electrochemical Science and Engineering, vol. 5, Wiley–VCH, Weinheim, 1997.
[88] R.F. Mann, J.C. Amphlett, B.A. Peppley, Frontiers Sci. Ser. 7 (1993) 613.
[89] R. Kumar, S. Ahmed, in: O. Savadogo, P.R. Roberge, T.N. Veziroglu (Eds.), New Materials for Fuel Cell Systems I, Les Éditions de l'École Polytechnique de Montréal, Montréal, Québec, Canada, 1995, p. 224.
[90] B.A. Peppley, J.C. Amphlett, R.F. Mann, in: W. Vielstich, A. Lamm, H.A. Gasteiger (Eds.), Handbook of Fuel Cells—Fundamentals Technology and Applications: Fuel Cells and Technology, vol. 3, Wiley & Sons, Chichester, 2003.
[91] F.A. Uribe, T. Zawodzinski Jr., S. Gottesfeld, The Electrochemical Society and the International Society of Electrochemistry Meeting, San Francisco, 2001, Conference abstract.
[92] R. Mohtadi, W.-K. Lee, S. Cowan, J.W. Van Zee, Electrochem. Solid State Lett. 6 (2003) A272.
[93] R. Mohtadi, W.-K. Lee, J.W. Van Zee, J. Power Sources 138 (2004) 216.
[94] F.A. Uribe, S. Gottesfeld, T.A. Zawodzinski, J. Electrochem. Soc. 149 (2002) A293.
[95] R. Halseid, Ph.D. Dissertation, Norwegian University of Science and Technology, 2004.
[96] R. Halseid, P.J.S. Vie, R. Tunold, Ninth Ulm Electrochemical Talks, 2004, Conference abstract.
[97] A.C.A. de Vooys, M.T.M. Koper, R.A. van Santen, J.A.R. Van Veen, J. Electroanal. Chem. 506 (2001) 127.
[98] X. Ren, T.E. Springer, S. Gottesfeld, J. Electrochem. Soc. 147 (2000) 92.
[99] W. Vielstich, V.A. Paganin, F.H.B. Lima, E.A. Ticianelli, J. Electrochem. Soc. 148 (2001) A502.
[100] J. Ling, O. Savadogo, J. Electrochem. Soc. 151 (2004) A1604.
[101] J. Zhang, T. Thampan, R. Datta, J. Electrochem. Soc. 149 (2002) A765.
[102] H.A. Gasteiger, S.S. Kocha, B. Sompalli, F.T. Wagner, Appl. Catal. B 56 (2005) 9.
[103] W. Vogel, J. Lundquist, P.N. Ross, P. Stonehart, Electrochim. Acta 20 (1975) 79.
[104] H. Kita, H. Naohara, T. Nakato, S. Taguchi, A. Aramata, J. Electroanal. Chem. 386 (1995) 197.
[105] K. Jambunathan, A.C. Hillier, J. Electroanal. Chem. 524–525 (2002) 144.
[106] H. Igarashi, T. Fujino, M. Watanabe, J. Electroanal. Chem. 391 (1995) 119.
[107] H.A. Gasteiger, N.M. Markovic, P.N. Ross, J. Phys. Chem. 99 (1995) 8945.
[108] N.M. Markovic, B.N. Grgur, C.A. Lucas, P.N. Ross, J. Phys. Chem. B 103 (1999) 487.
[109] N.M. Markovic, C.A. Lucas, B.N. Grgur, P.N. Ross, J. Phys. Chem. 103 (1999) 9616.
[110] I. Langmuir, J. Am. Chem. Soc. 40 (1918) 1361.
[111] At 1.2 V the CO oxidation rate is lower than the CO adsorption rate at 0.06 V, which is reflected also by the decay in oxidation rate at potentials positive of 0.9 V due to oxide formation. See Refs. [76,126,139,140].
[112] M.W. Roberts, C.S. McKee, Chemistry of the Metal–Gas Interface, Clarendon Press, Oxford, 1978.
[113] P.J. Kisliuk, J. Phys. Chem. Solids 3 (1957) 95.
[114] P.J. Kisliuk, J. Phys. Chem. Solids 5 (1958) 78.
[115] R.J. Bellows, E.P. Marucchi-Soos, D.T. Buckley, Ind. Eng. Chem. Res. 35 (1996) 1235.
[116] D. Kardash, J. Huang, C. Korzeniewski, Surf. Sci. 476 (1999) 95.
[117] D. Kardash, J. Huang, C. Korzeniewski, Langmuir 16 (2000) 2019.
[118] E. Herrero, J.M. Feliu, S. Blais, Z. Radovic-Hrapovic, G. Jerkiewicz, Langmuir 16 (2000) 4779.
[119] E. Herrero, B. Alvarez, J.M. Feliu, S. Blais, Z. Radovic-Hrapovic, G. Jerkiewicz, J. Electroanal. Chem. 567 (2004) 139.
[120] T. Kawaguchi, W. Sugimoto, Y. Murakami, Y. Takasu, Electrochem. Commun. 6 (2004) 480.
[121] M. Kawasaki, H. Nagayama, Surf. Sci. 549 (2004) 237.
[122] L. Palaikis, D. Zurawski, M. Hourani, A. Wieckowski, Surf. Sci. 199 (1988) 183.
[123] D. Zurawski, M. Wasberg, A. Wieckowski, J. Phys. Chem. 94 (1990) 2076.
[124] B. Rush, J.A. Reimer, E.J. Cairns, J. Electrochem. Soc. 148 (2001) A137.
[125] T. Iwasita, U. Vogel, Electrochim. Acta 33 (1988) 557.

[126] G. Jerkiewicz, G. Vatankhah, J. Lessard, M.P. Soriaga, Y.-S. Park, Electrochim. Acta 49 (2004) 1451.
[127] C. Plog, Verfahren zur katalytischen Entfernung von CO in H_2-reichem Gas, German Patent 650 922 A1 (1994).
[128] D.P. Wilkinson, H.H. Voss, K.B. Prater, G.A. Hards, T.R. Ralph, D. Thompsett, Electrode comprising first and second catalytic component, European Patent EU EP0736921A1 (1996).
[129] D.P. Wilkinson, D. Thompsett, in: O. Savadogo, P.R. Roberge (Eds.), New Materials for Fuel Cell and Modern Battery Systems, vol. II, Ecole Polytechnique de Montreal, Montreal, 1997, pp. 266–285.
[130] L.P.L. Carrette, K.A. Friedrich, M. Huber, U. Stimming, Phys. Chem. Chem. Phys. 3 (2001) 320.
[131] M.J. Kahlich, H.A. Gasteiger, R.J. Behm, J. Catal. 171 (1997) 93.
[132] C. Sishtla, G. Koncar, R. Platon, S. Gamburzev, A.J. Appleby, O.A. Velev, J. Power Sources 71 (1998) 249.
[133] F.A. de Bruijn, D.C. Papageorgopoulos, E.F. Sitters, G.J.M. Janssen, J. Power Sources 110 (2002) 117.
[134] T. Smolinka, U. Wittstadt, W. Lehnert, in: D. Stolten, B. Emonts, R. Peters (Eds.), Proceedings of the Second European Fuel Cell Forum, European Fuel Cell Forum, Luzern, 2003, pp. 263–270.
[135] T. Diemant, T. Hager, H.E. Hoster, H. Rauscher, R.J. Behm, Surf. Sci. 541 (2003) 137.
[136] N. Bronstedt, Chem. Rev. 5 (1928) 231.
[137] U. Koponen, T. Peltonen, M. Bergelin, T. Mennola, M. Valkiainen, J. Kaskimies, M. Wasberg, J. Power Sources 86 (2000) 261.
[138] C.L. Green, A. Kucernak, J. Phys. Chem. B 106 (2002) 11446.
[139] G. Jerkiewicz, G. Vatankhah, A. Zolfaghari, J. Lessard, Electrochem. Commun. 1 (1999) 419.
[140] K. Jambunathan, A.C. Hillier, J. Electroanal. Chem. 524–525 (2002) 144.